
Article:
Mäkelä, R., Arjonen, A., Suryo Rahmanto, A. et al. (7 more authors) (2020) Ex vivo assessment of targeted therapies in a rare metastatic epithelial–myoepithelial carcinoma. Neoplasia, 22 (9). pp. 390-398. ISSN 1476-5586

https://doi.org/10.1016/j.neo.2020.06.007

NEOPLASIA
www.neoplasia.com
Volume 22 Number 9 September 2020 pp. 390–398

Ex vivo assessment of targeted therapies in a rare metastatic epithelial–myoepithelial carcinoma

Rami MÌkelÌ [a]; Antti Arjonen [a]; Aldwin Suryo Rahmanto [b]; Ville HÌrmÌ [a,c]; Janne LehtiÎ [d]; Teijo Kuopio [e]; Thomas Helleday [c]; Olle Sangfelt [b]; Juha Kononen [e,f]; Juha K. Rantala [a,c,*]

[a] Misvik Biology Oy, Turku, Finland; [b] Karolinska Institutet, Department of Cell and Molecular Biology, Stockholm, Sweden; [c] University of Sheffield, Department of Oncology and Metabolism, South Yorkshire, Sheffield, UK; [d] Department of Oncology-Pathology, Science for Life Laboratory, Karolinska Institutet, Stockholm, Sweden; [e] Central Finland Health Care District, JyvÌskylÌ Medical Centre, JyvÌskylÌ, Finland; [f] Docrates Hospital, Helsinki, Finland

Abstract

Epithelial–myoepithelial carcinoma (EMC) is a rare subtype of salivary gland neoplasms. Since the initial description of the cancer, just over 300 cases have been reported. EMCs occupy a biphasic cellular differentiation-state defined by the constitution of two cell types representing epithelial and myoepithelial lineages, yet the functional consequence of the differentiation-state heterogeneity with respect to therapy resistance of the tumors remains unclear. The reported local recurrence rate of the cases is approximately 30%, and while distant metastases are rare, a significant fraction of these cases are reported to receive no survival benefit from radio- or chemotherapy given in addition to surgery. Moreover, no targeted therapies have been reported for these neoplasms. We report here the first use and application of *ex vivo* drug screening together with next generation sequencing to assess targeted treatment strategies for a rare metastatic epithelial–myoepithelial carcinoma. Results of the *ex vivo* drug screen demonstrate significant differential therapeutic sensitivity between the epithelial and myoepithelial intra-tumor cell lineages suggesting that differentiation-state heterogeneity within epithelial–myoepithelial carcinomas may present an outlet to partial therapeutic responses to targeted therapies including MEK and mTOR inhibitors. These results suggest that the intra-tumor lineage composition of EMC could be an important factor to be assessed when novel treatments are being evaluated for management of metastatic EMC.

Neoplasia (2020) 22 390–398

Keywords: Epithelial–myoepithelial carcinoma, Personalized medicine, Ex vivo drug screening, Targeted therapy, Cancer diagnostics

Introduction

Epithelial–myoepithelial carcinoma (EMC) of the salivary gland is a rare type of cancer that account for 0.4 to 1.5% of all salivary gland tumors. Initial pathological description of EMC was published in 1972 [1], and the largest worldwide review of cases has covered 246 cases [2]. Altogether some 350 cases of EMC have been reported in the literature. The tumorigenesis of these rare cancers is largely unclear, but the single common feature of the cancer is the histological biphasic morphology composed of epithelial and myoepithelial cell lineages defining the key histologic characteristic finding used in the diagnosis of EMC (Fig. 1A). Clinically, local EMC has been described as a low-grade neoplasm that progresses slowly. The tumors are most commonly arising from the parotid glands and to lesser extent from submandibular or minor salivary glands. Histologically the EMC neoplasms consists of both epithelial and myoepithelial cells arranged in differentiated ductal tubules, trabeculae, small islands or sheets with varying differentiations, but commonly no or little invasion to surrounding tissues. Although the reported local recurrence rate of EMC is up to 30–40% [2,3], mortality of EMC is low [2,4], despite for the rare metastatic disease to which no curative treatment is available [2,5]. The mainstay of treatment of EMC carcinomas consists of surgery with up to 97% of patients described in literature going through surgery [2]. Due to the low number of cases, no large randomized trials

Abbreviations: EMC, Epithelial–myoepithelial carcinoma, HCA, High content assay, RPPA, Reverse phase protein arrays

* Corresponding author at: Misvik Biology, Karjakatu 35 B, FI-20520 Turku, Finland. e-mail addresses: makela@misvik.com (R. MÌkelÌ), arjonen@misvik.com (A. Arjonen), aldwin.suryo.rahmanto@ki.se (A. Suryo Rahmanto), v.harma@sheffield.ac.uk (V. HÌrmÌ), janne.lehtio@ki.se (J. LehtiÎ), teijo.kuopio@ksshp.fi (T. Kuopio), olle.sangfelt@ki.se (O. Sangfelt), juha.kononen@docrates.com (J. Kononen), rantala@misvik.com (J.K. Rantala).

https://doi.org/10.1016/j.neo.2020.06.007

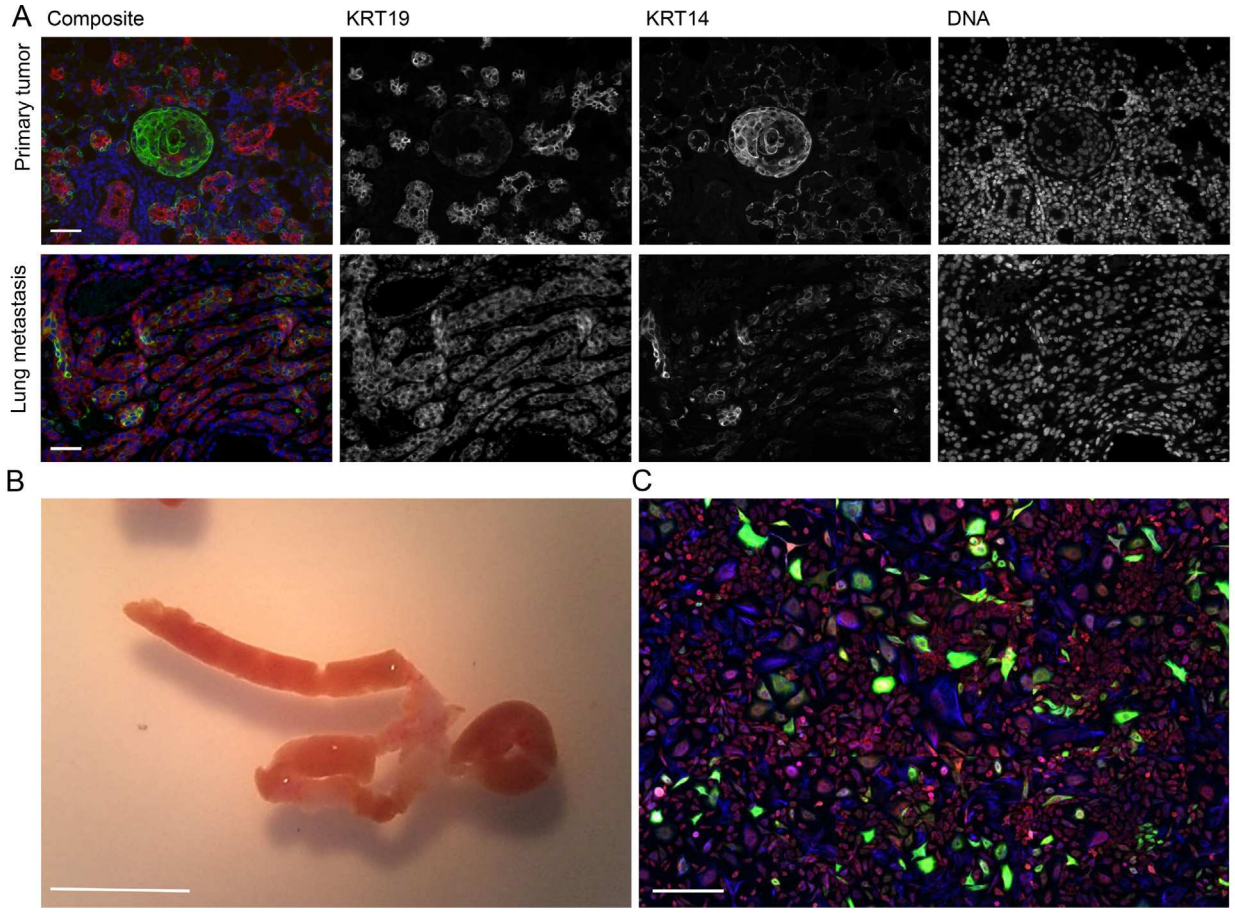

Fig. 1. Histological comparison of the patient's primary tumor, the lung metastasis and cell culture. (A) Immunofluorescent staining of KRT19 (red) and KRT14 (green) in the patient¨s primary tumor and the lung metastasis tissue. DNA shown in blue. Bars 50 μm. (B) Two 18-gauge needle biopsy cores were used to establish an *ex vivo* cell culture for the drug screening. Bar 1 mm. (C) Immunofluorescent staining of KRT19 (red), KRT14 (green) and Vimentin (blue) in the ex vivo tumor cell culture. Bar 50 μm.

have been performed for EMC and the role of e.g. adjuvant radiotherapy and chemotherapy after surgery is not clearly defined. Thus, systemic therapy for recurrent and/or metastatic EMC is generally based on standard cytotoxic drugs such as doxorubicin, cisplatin, 5-fluorouracil, paclitaxel and navelbine [6–8]. Given the rarity of metastatic EMC tumors and the variability in nature of the metastatic disease, the survival benefits of cytotoxic agents in treatment of EMC has not been defined and the reported clinical responses have been short in duration. Therefore, there is a need for better understanding of the complex biology of epithelial–myoepithelial carcinoma, and to develop therapeutic approaches considering the cellular heterogeneity of the tumors and the underlying genetic background such as the frequent association of EMC with Harvey rat sarcoma viral oncogene homolog (*HRAS*) mutations [9–11].

In this study, we report the first use of *ex vivo* analysis of drug sensitivity for a rare metastatic EMC case to inform the treatment of the patient after the standard treatments had been exhausted. Use of high-throughput *ex vivo* drug screening [12–14] is an attractive application for biomarker discovery and assessment of patient specific therapy sensitivity especially for rare cancers for which large-scale clinical trials of novel therapies are challenging due to low number of cases [15]. To assess sensitivity of the patient derived EMC cells to targeted cancer therapeutics, we present the utility of a pathological marker informed high-content assay (HCA) strategy to track epithelial and myoepithelial sub-cell populations through immunofluorescent markers in an *ex vivo* -high content drug screen. Our findings elucidate how EMC tumor derived cells with pronounced differentiation-state heterogeneity respond to specific targeted pathway antagonism at single cell resolution, revealing dramatic differentiation state selectivity for pathway-targeted drugs. Using these methods to understand how pharmacologic pathway antagonism affects the intra-tumoral heterogeneity in EMC, we may begin to predict the phenotypic responses of patients¨ tumor cells to therapy *in vivo*, and thus design drug combinations and new indications for currently existing targeted cancer therapeutics to treat metastatic EMC.

Materials and methods

Patient

The patient, a 36-year old female, was identified to the study by an oncologist at the Tampere University Hospital (Tampere, Finland). The patient was initially diagnosed at age of 32 when radical surgery of the salivary gland was performed. Diagnosis was myoepithelial–epithelial carcinoma of the salivary gland. Whole-body CT (computerized tomography) scan indicated no distant disease spread and patient was considered cured of the disease and she received no additional adjuvant treatment. At age of 36 the patient was diagnosed with multiple small metastatic disease nodules in the right lung and two large intrapulmonary metastatic lesions which were biopsied to obtain diagnosis. Tissue morphology was similar to the primary tumor (Fig. 1A). Metastases were inoperable and patient was referred for systemic

therapy. First line chemotherapy consisted of cisplatin, docetaxel and 5-fluorouracil. Clinically, she did not benefit from the treatment and objective response evaluation with whole-body CT imaging after three cycles indicated clear disease progression. The patient was then considered for detailed molecular pathology profiling and the *ex vivo* therapy sensitivity study. Needle biopsy samples were collected for the *ex vivo* drug screening and DNA sequencing with approval from the local Ethics Committee of the Central Finland Health Care District (KSSHP 3U/2015). All the experiments were undertaken with the understanding and written informed consent of the patient and the study methodologies conformed to the standards set by the Declaration of Helsinki.

Tissue specimens

FFPE histological specimens from the patient's primary tumor were available for the study from the time of initial diagnosis and surgical resection of the tumor with clinical follow-up data available. Four 18-gauge coarse needle biopsy cores from metastatic lesion in the right lung were collected for the next generation sequencing and *ex vivo* drug screening experiments.

Tumor derived primary cell culture

Two of the four 18-gauge coarse needle biopsy cores sampled from the metastatic lesion were devoted to establish a vital cell culture from the patient's tumor cells. The tissue cores were placed in sterile RMPI-1640 medium (Gibco) without supplements for transport to the research laboratory (Fig. 1B). One needle core was fixed in 4% buffered formaldehyde, paraffin-embedded, cut at 4 µm, and subjected to routine histological staining procedures as well as fluorescence immunocytochemistry (Fig. 1A). Immediately upon receipt, the live tissue samples were washed three times with sterile PBS and finely cut to 2–5 mm [3] pieces in sterile cell culture medium using scalpels. The primary bulk cell suspension dissociated from the tumor tissue during cutting was collected into a sterile centrifuge tube. The remaining tissue fractions where then placed into 1 mL of Accutase cell dissociation reagent (Gibco) per tissue and incubated at room temperature for 60 minutes. Following the enzymatic dissociation, the resulting cell suspensions and the initial cell suspension from the tissue cutting plates were combined, collected with centrifugation and subjected to filtration through a 70 µm cell strainer (pluriSelect Life Science UG) in sterile RMPI-1640 medium. The resulting cell suspension was quantified using a Cellometer Mini cell counter (Nexcelom). In total 2.5 × 10^6 cells with an average size of >13 µm was derived from the tumor tissue. The suspension was diluted to RPMI-1640 medium containing 5% FBS to achieve a suspension with 1000 cells per 45 µL of medium. 10^6 cells were used for the initial *ex vivo* drug screening and the rest were placed to cell culture in standard cell culture conditions (37 °C, 5% CO_2). Following four days in culture, the cells presented an adherent phenotype with distinct sub-cell populations representing the tumor tissue (Fig. 1C).

Mutation analysis

The genomic profiling was purchased as a service from the Finnish Institute for Molecular Medicine (FIMM) Genomic Core (Helsinki, Finland). Briefly, genomic DNA was isolated from two fresh 18-gauge coarse needle biopsy cores using the Epicentre Master pure DNA and RNA isolation kit (Illumina) according to the manufacturer's protocol. Germline DNA was obtained from a non-cancerous skin biopsy. Exome capture was performed using Nextera Rapid Capture Exome Kit (Illumina). Sequencing libraries were sequenced using paired end 100 bp read format on an Illumina HiSeq2500 instrument (Illumina). Result of the mutation analysis are provided in the Supplementary Data 1.

Immunostaining of tissue samples

The primary and metastatic tumor tissue samples were formalin-fixed, paraffin-embedded and cut sections were prepared with pathologist assistance. For immunofluorescence staining 5 µm cut sections were deparaffinized in xylene and passed through a series of graded alcohols. Antigen retrieval was performed in a 0.1 M sodium citrate buffer pH 6 (Sigma) under heat and pressure, followed by blocking with a 1% BSA (ThermoFisher) blocking buffer. Sections were incubated overnight at 4 °C with a primary antibody solution with epithelial marker cytokeratin-19 (KRT19, Dako, Clone RCK108), 1:300), myoepithelial marker cytokeratin-14 (KRT14, Abcam, Clone LL002, 1:300) and proliferating cell marker Ki-67 (DAKO, Clone MIB-1, 1:200) diluted in 1% BSA. Sections were washed in PBS with 0.1% Tween (ThermoFisher) and secondary antibody staining was performed at room temperature for 1 hour with AlexaFluor secondary antibodies against primary host species (1:500, LifeTech) in 1% BSA. 1 µg/ml DAPI (4′,6-Diamidino-2-phenylindole nuclear counterstain, LifeTech) was added to secondary staining buffers. Tissue sections were imaged on an Olympus scan^R platform at 20× magnification.

Image-based drug screening

The therapeutic compound collection used in the *ex vivo* study consisted of 134 FDA approved anti-cancer agents, along with 12 investigational compounds covering key cancer associated signaling pathway targets (Supplementary data 2). The compounds were purchased from commercial chemical vendor (Selleck biochemicals) readily dissolved in dimethyl sulfoxide (DMSO). Platinum based compounds were dissolved in water. The *ex vivo* drug screening was performed in tissue culture treated 384-well microplates (Corning CellBIND, #3770). Each compound was tested in four different concentrations with 2-fold dilutions starting from 5 micromolar as the highest. A single-cell suspension of freshly isolated tumor cells (45 µl per well; 1000 cells per well) was transferred to each well using a peristaltic dispenser (ThermoScientific). The 384-well plates were incubated for 96 h at standard cell culture conditions. Analysis of cell viability with cellular lineage separation was performed through high-content imaging. The cell cultures were fixed and stained as detailed above (Immunostaining of tissue samples) with antibodies against epithelial KRT19 (1:300), myoepithelial KRT14 (1:300) and DAPI for DNA counterstaining. Cells were imaged on the Olympus scan^R platform at 10× magnification. 6 frames were acquired from each 384-well. Images were analyzed with Olympus scan^R image analysis suite including DNA staining-based primary object segmentation using a watershed algorithm. Primary objects (nuclei) were expanded a fixed 10-pixel distance, and mean fluorescence signal intensity for KRT19 and KRT14 was quantified from this expanded cellular region. Single cell positivity for KRT19 and KRT14 were determined by gating in the scan^R image analysis suite, using cells negative for each marker as controls. Population separated cell count data was normalized to DMSO-only wells (negative control), 5 µM staurosporin-containing wells (positive control) and 2 µM aphidicolin-containing wells (cell growth control). Dose response curves for growth rate normalized GR50, IC50, maximal inhibition (Emax) and the projected maximal inhibition (Einf) estimates were generated in GraphPad Prism software (V7, GraphPad Software Inc.).

Statistical analysis

The *ex vivo* drug screening data was analyzed using the normalized growth rate inhibition (GR) approach which yields per-division metrics for drug potency (GR50) and efficacy (GRmax). The normalized growth rate inhibition (GR) method corrects for variation in division rates by estimating the magnitude of drug response on a per cell-division basis

[13,14]. For analysis of variation in cell lineage heterogeneity following drug treatments we used the Shannon diversity index as a metric of cell-state heterogeneity. Cell state frequencies were calculated using the Olympus scan^R imaging cytometry software (Olympus OSIS, Germany) as described above. For each drug treatment, the proportion of each cell state (P_i) was calculated by dividing cell state number by the total cell number in the well. The Shannon diversity index (H') was then calculated by multiplying P_i by the $\log_2$ of P_i, for each cell state, then summing these numbers for the total number of states (S).

$$H' = -\sum_{i=1}^{2} P_i ln P_i$$

Combination indices (CI) were calculated from replicate, fixed-ratio, dose escalation experiments using the Chou and Talalay method [17]. CI values were reported at 50% inhibitory values (CI50). Welch's *t*-test and Pearson correlation analyses were applied using GraphPad Prism V7 software as indicated in the figure legends according to assumptions on data normality.

Results and discussion

Image-based ex vivo drug efficacy screening

The patient was initially treated with radical surgery of the affected salivary gland. Adjuvant treatment of the patient following metastatic relapse consisted of three cycles of chemotherapy with cisplatin, docetaxel and 5-fluorouracil. The disease progressed immediately through the adjuvant chemotherapy. At this stage, coarse needle tumor biopsies were received for the purpose of genetic profiling and *ex vivo* therapy efficacy screening. For the *ex vivo* drug screening experiment the tissue samples were processed immediately on the day of biopsy. Using standard techniques to establish primary cell cultures from human tissues [18], a primary culture was prepared from the patient's tumor tissue. This bulk tumor cell sample was then used for a high content drug screen to assess the relative lineage specific cytotoxicity of 146 drugs representing various anti-cancer drug classes with a fixed dose range (Supplement data 2). Cells were exposed to the drugs for 96 h and automated microscopy and image analysis were used to quantify cell growth on basis of cell counting following staining with lineage specific intermediate filament markers KRT19 and KRT14 (Fig. 1A). Aphidicolin was used as a reference molecule to monitor and normalize the dose responses with respect to growth rate (GR) during the assay. With comparison of the negative control samples (DMSO only) and aphidicolin treated cells, the estimated cell doubling rate of all the tumor tissue derived cells was calculated to be 34 h corresponding [19] (Fig. 2A). ~70% of the cells in control conditions were positive for the epithelial lineage marker KRT19. Cell division rate of the KRT19$^+$ cells was calculated to be 24 h corresponding to 4 cell division over the course of the assay. ~17% of the cells were positive for the myoepithelial lineage marker KRT14. Cell division rate of the KRT14$^+$ cells was calculated to be 56 h (Fig. 2A). The differential proliferation rate of the two different cell lineages reflected the population specific Ki67 index in the lung metastasis tissue where the measured Ki67 index of KRT19$^+$ cells was 19% and 12% for KRT14$^+$ cells (Supplement Fig. 1A). To identify the most potent growth inhibitory drugs, we compared the GR values of the drugs calculated separately for the KRT19$^+$ cells, KRT14$^+$ cells and all cells (Fig. 2B, Supplement Fig. 2). The GR metrics were combined with analysis of changes in the diversity of proportional lineage heterogeneity measured using a Shannon diversity index score [16] to identify lineage specificity in the drug efficacy (Fig. 2B). Using a stringent ranking criterion where the average of the GR values across all four drug doses had to be stronger than GR = 0 (the cell growth stalling effect of aphidicolin), we identified 21 drugs associated with strong a cytotoxicity effect on all the cells, 30 drugs with strong cytotoxicity on the KRT19$^+$ cells and 36 drugs with strong cytotoxicity on the KRT14$^+$ cells (Supplement Fig. 3). The overall drug efficacy results (IC_{50}) of all the drugs correlated best between the faster proliferating KRT19$^+$ cells and analysis of all the cells (Pearson correlation $r = 0.98$). The correlation of the IC50 results between KRT19$^+$ and KRT14$^+$ cells displayed significant variation for selected drugs enriched for mTOR, MEK, HDAC and DHFR (dihydrofolate reductase) inhibitors ($r = 0.86$) (Fig. 2C, Supplement Fig. 2). To identify the drugs with most differential efficacy between the two cell lineages, we performed a pairwised correlation analysis of the growth rate normalized dose responses of the KRT19$^+$ and KRT14$^+$ cells. From the pathway targeted therapeutics, the GR dose response profiles of drugs against mTOR, MEK, Bcr-Abl, HDAC, PDGFR and Raf had a strong negative correlation between the two cell lineages ($r < -0.5$) reflecting differential growth inhibitory efficacy dependent on the lineage state (Fig. 2D). From this list of drugs, the GR dose response difference was statistically most significant (Welch's *t* test) for MEK inhibitor AZD6244 (Selumetinib), Raf inhibitor AZ628, HDAC inhibitor Vorinostat, MEK inhibitor Trametinib, mTOR inhibitor Temsirolimus and mTOR inhibitor AZD8055 (Fig. 2E).

Analysis of lineage selective growth inhibition

The microscopy-based assay strategy allows detailed analysis of changes in total cell numbers, cell cycle distribution, and sub-cell lineage marker identified population dynamics at single-cell resolution. The multiparameter data can thus be used to discover and assess drug induced changes through multiple phenotypes. As an example, drug induced effects on cell cycle distribution can be analyzed with imaging cytometry [20] and used to group drugs and drug classes according to cell cycle arresting features (Supplement Fig. 4). With analysis of the epithelial and myoepithelial lineage specific growth inhibitory effects, we identified several drugs that induced dose-dependent alterations on the diversity of the sub-cell lineages, resulting in unique differentiation-state distributions in residual cell populations following treatment (Fig. 3A). Overall, the lineage specific drug responses could be grouped into four main classes: drugs having a cytotoxic effect on all the cells, drugs more potent on the KRT19$^+$ population, drugs more potent on the KRT14$^+$ population and drugs increasing growth of both two lineages (Supplement Fig. 5). Interestingly, drugs with same therapeutic targets grouped within these response classes. For example, inhibitors targeting the PI3K/mTOR pathway, dose-dependently decreased viability of KRT14$^+$ cells while KRT19$^+$ cell were more resistant (Fig. 3A). Conversely, inhibitors targeting the MAP-Kinase (MAPK) pathway, including MEK and BRaf inhibitors, and HDAC inhibitors displayed higher efficacy on the KRT19$^+$ cells in comparison to KRT14$^+$ cells (Fig. 3A). To expand the grouping of drugs according to lineage selectivity, we compared the change in the proportional amount of KRT19$^+$ vs. KRT14$^+$ cells in the residual population following drug treatment using the Shannon diversity index H' metric. We calculated the change in the overall diversity index ($\Delta H'$) by comparing the residual population indices to the H' index of DMSO only control samples (Fig. 3B). Here several other drugs were identified having a similar lineage specific effect as the MEK and mTOR inhibitors. Drugs having a myoepithelial lineage selective effect included e.g. Niclosamide, Vinblastine and Docetaxel. The differential growth inhibitory effects of these groups of drugs on the two cell populations is shown in Fig. 3C displaying the GR dose response curves of the two populations. The impact to the same drugs on the proportional lineage diversity is shown in Fig. 3D as % change of the proportional cell population size in comparison to DMSO controls. Strikingly, the MEK inhibitors increased the proportional amount of KRT14$^+$ cells up to 4-fold similarly as Vinblastine, Raf inhibitor AZ628 and Calcitriol (Fig. 3D).

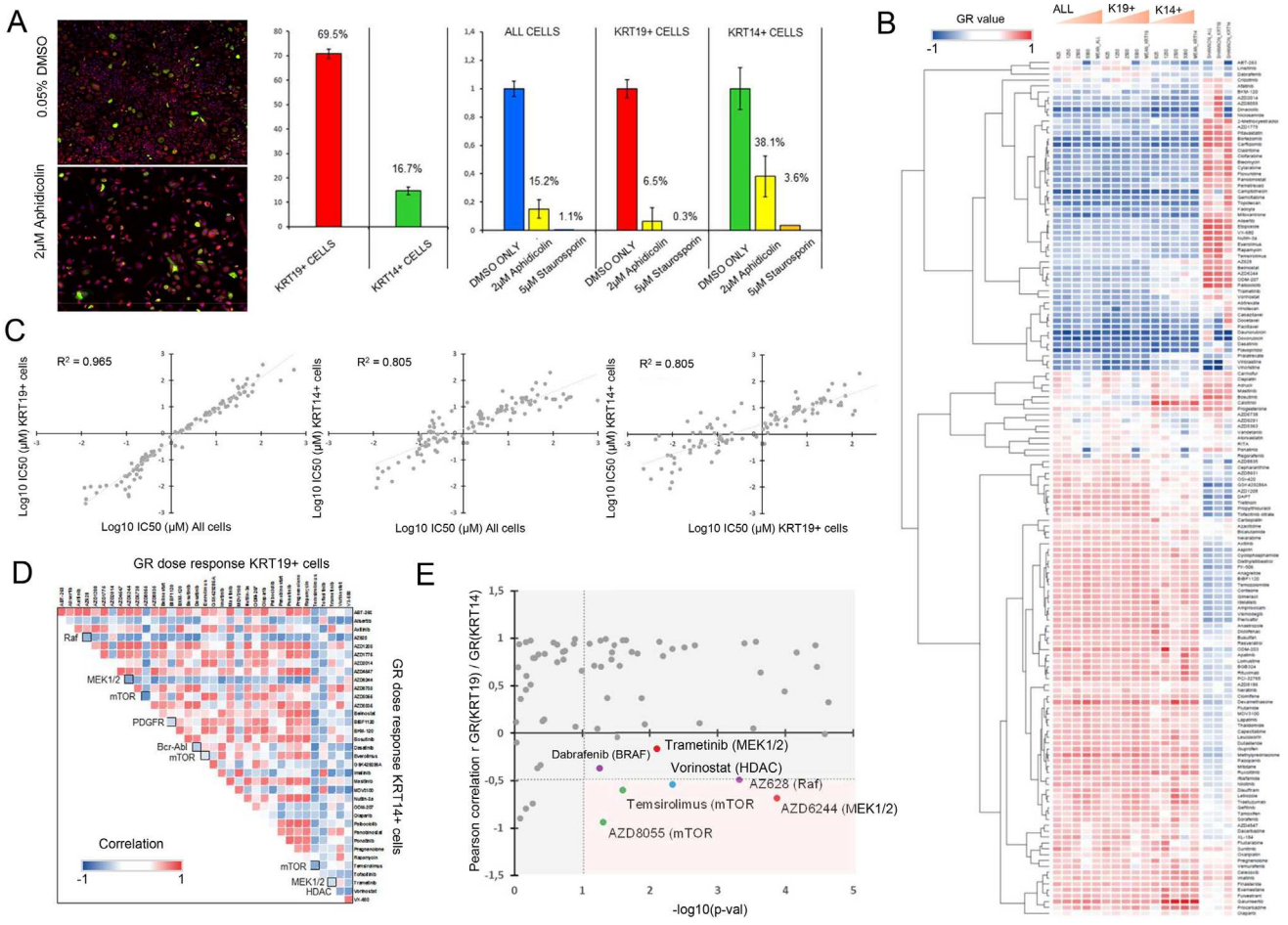

Fig. 2. Ex vivo high content imaging drug screening. (A) Growth rate normalization of the dose responses was applied using aphidicolin as a cell growth stalling control agent. In the *ex vivo* cell culture ~70% of cells expressed KRT19 and ~17% KRT14. The calculated cell doubling rate was measured for all cells and KRT19/KRT14 positive cells separately. (B) A heatmap visualization of the GR value scored dose responses for all cells, KRT19$^+$ cells and KRT14$^+$ cells. Shannon diversity index measurements were used to score divergent effects of the drugs to epithelial and myoepithelial cells. (C) Correlations of the IC50 estimates of all the growth modulating drugs between all cells and KRT19$^+$/KRT14$^+$ cells and KRT19$^+$ vs. KRT14$^+$ cells. (D) Correlation matrix of the GR dose response profiles of the most effective targeted agents identified by the drug screening between KRT19$^+$ and KRT14$^+$ cells. Pearson correlation value r indicated with the intensity of the color. Red positive correlation, blue negative correlation. (E) Scatter plot showing the correlation of the lineage specific GR dose response correlations and the significance ($-\log_{10}p$-val, Welch's *t* test).

Combination of pathway targeted therapeutics

To analyze pathway inhibition and target engagement of the identified drug candidates, we performed a high-throughput reverse-phase-protein array (RPPA) screen with the patient¨s cells [21]. In the RPPA analysis the cells were exposed for 72 h to a collection of 58 drugs selected from the initial *ex vivo* analysis in 5 doses with 2-fold dilutions starting from 5 μM (Supplement data 3). Nine markers; phospo-p70S6R, phospho-AKT, phospho-ERK, phospho-4EBP1, phospho-EIF4G, phospho-Chk1, Ki-67 and EMA (MUC1) were used as the assay readout (Supplement Fig. 5A). Molecular pathway analysis of the downstream signaling markers confirmed a strong correlation between the viability of the EMC cells and the engagement of each of the targeted inhibitors on their targets for the PI3K/AKT/mTOR, and the RAS/RAF/MEK pathways (Supplement Fig. 5B). Drugs including MEK inhibitor selumetinib and HDAC inhibitors effectively blocked downstream p-ERK1/2 signaling, while mTOR, PI3K, AKT and CDK inhibitors had a marked dose dependent reduction in downstream mTORC1/2 effectors p-AKT, p-S6RP and p-4EBP1. CDK inhibition and WEE1 inhibitor AZD1775 resulted in significant dose dependent induction of DNA damage marked by increased γH2Ax positivity and downregulated p-Chk1 S345 (Supplement Fig. 5A).

Supported by the pathway inhibition analysis and the apparent differential sensitivity of the KRT19$^+$ and the KRT14$^+$ cells on MAPK/mTOR pathway inhibition, we rationalized that combination of MEK and mTOR inhibition should potentiate the overall therapeutic efficacy of the single agents. We explored the effects of combining two of the highest-ranking drugs with a divergent growth inhibitory effect; MEK inhibitor AZD6244 (Selumetinib) and mTORC1/2 inhibitor AZD2014 (Vistusertib). Patient cells were treated for 96 h with the two inhibitors in a dose–response matrix to identify synergistic relationships of the two drugs (Fig. 4A). At equal molar ratio of 1:1, the combination showed significant additive effects (CI50 Combination index: 0.22) of reducing cell proliferation and increasing apoptosis resulting in a net reduction in cell numbers of both lineages following 96 h of treatment (Fig. 4A & 4B). Analysis of the synergy of the drug combinations with the other drug kept at a fixed dose revealed higher synergistic behavior of AZD2014 in low doses when

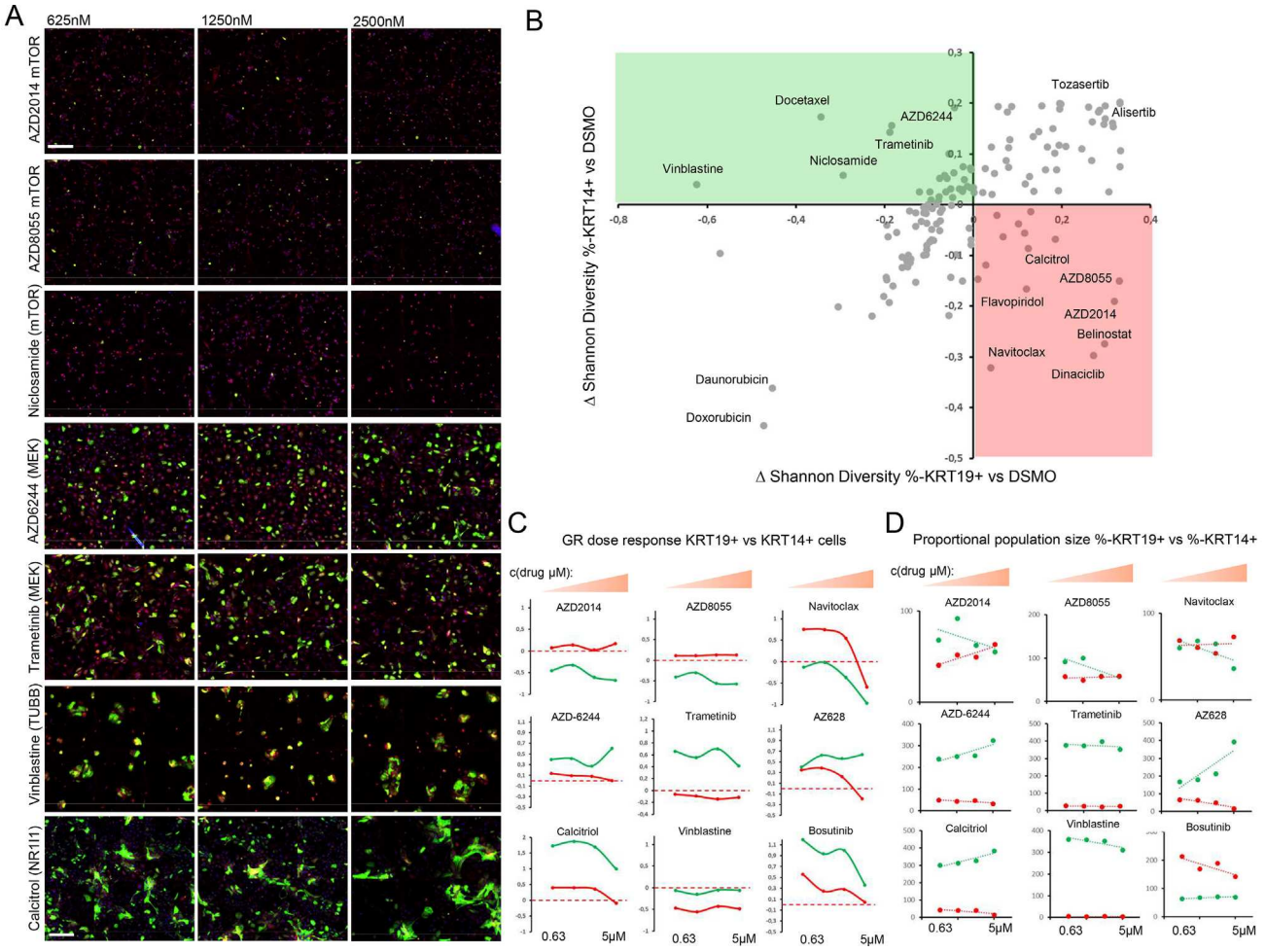

Fig. 3. Lineage specific drug responses. (A) Gallery views of the or screening samples for the drugs with the strongest divergent growth inhibitory effect on the KRT19$^+$ and KRT14$^+$ EMC cells. KRT19 shown in red, KRT14 shown in green and DNA blue. Bars 100 μm. (B) Scatter plot showing the correlation of the drug induced Shannon diversity index changes ($\Delta H^{'}$) in the KRT19$^+$ and KRT14$^+$ cell populations. Drugs highlighted with red increased the proportional amount of KRT19$^+$ cells in the screen and drugs highlighted in green increased the proportional amount of KRT14$^+$ cells in the screen. (C) Comparison of the lineage specific GR dose response curves for the KRT19$^+$ (red) and KRT14$^+$ (green) populations. (D) Visualization of the proportional changes of the KRT19$^+$ and KRT14$^+$ population sizes following exposure to the drugs in an increasing dose.

combined with AZD6244 than AZD6244 when combined with AZD2014 (Fig. 4A). Scaled-up replicate experiments for analysis of the target engagement and lineage inhibition of the combination was validated with conventional immunoblot analysis (Fig. 4C). Specifically, the combination of AZD6244 and AZD2014 resulted in high efficacy inhibition of the mTORC1 and S6 ribosomal protein suggesting the combination to may overcome the negative feedback of mTORC1/S6 kinase1 feedback loop described in several cancer models [22–24].

Ex vivo informed treatment

For EMC, there is no second-line treatment guidelines and no suitable clinical trials existed for this tumor type. Therefore, patient was considered for experimental therapeutic approaches informed by the *ex vivo* screening. Based on the drug screening results, the patient¨s tumor cells were highly sensitive in a differentiation state dependent manner to MEK and mTOR inhibition. These results could also be associated with findings from the whole exome sequencing of the tumor tissue. Key oncogenic aberrations discovered in the patient tumor cells included mutations in ARID1B, ATR (I774N), ERBB4 (V298G), HRAS (G13R), MAPK1 (AG7G), PIK3R1 (RE461Q), PIK3R1 (L244*) and RPTOR (W1313G) (Supplement data 1, Table 1).

Both HRAS and PIK3R1 mutations are associated based on *in vitro* and *in vivo* evidence with increased sensitivity of cancer cells to MEK inhibition [25,26]. Mutations in PI3KR1 gene coding for p85α, the regulatory subunit of PI3K, may also convert sensitivity to targeted PI3K and downstream effector inhibition including AKT and mTOR [27]. Mutations of RPTOR are associated with *in vivo* activity of mTOR inhibition and partial response to inhibition of MEK [28]. Based on these and the *ex vivo* results and after unsuccessful search of available clinical trials for mTOR-MEK combination therapies, the patient was started on Everolimus mTOR inhibitor therapy at a daily 10 mg dose adopted from renal cell cancer indication. Clinical benefit from this therapy was apparent already at the first control one month after initiation of therapy. Radiographic examination indicated initially a ∼25% reduction of the diameter of the largest metastatic disease lesions (Fig. 5). Further follow-up whole-body CT scans showed that the disease remained stable for 11 months under the Everolimus therapy. At the time of disease progression, a new subcutaneous metastatic lesion appeared in right mid-axillary line. A

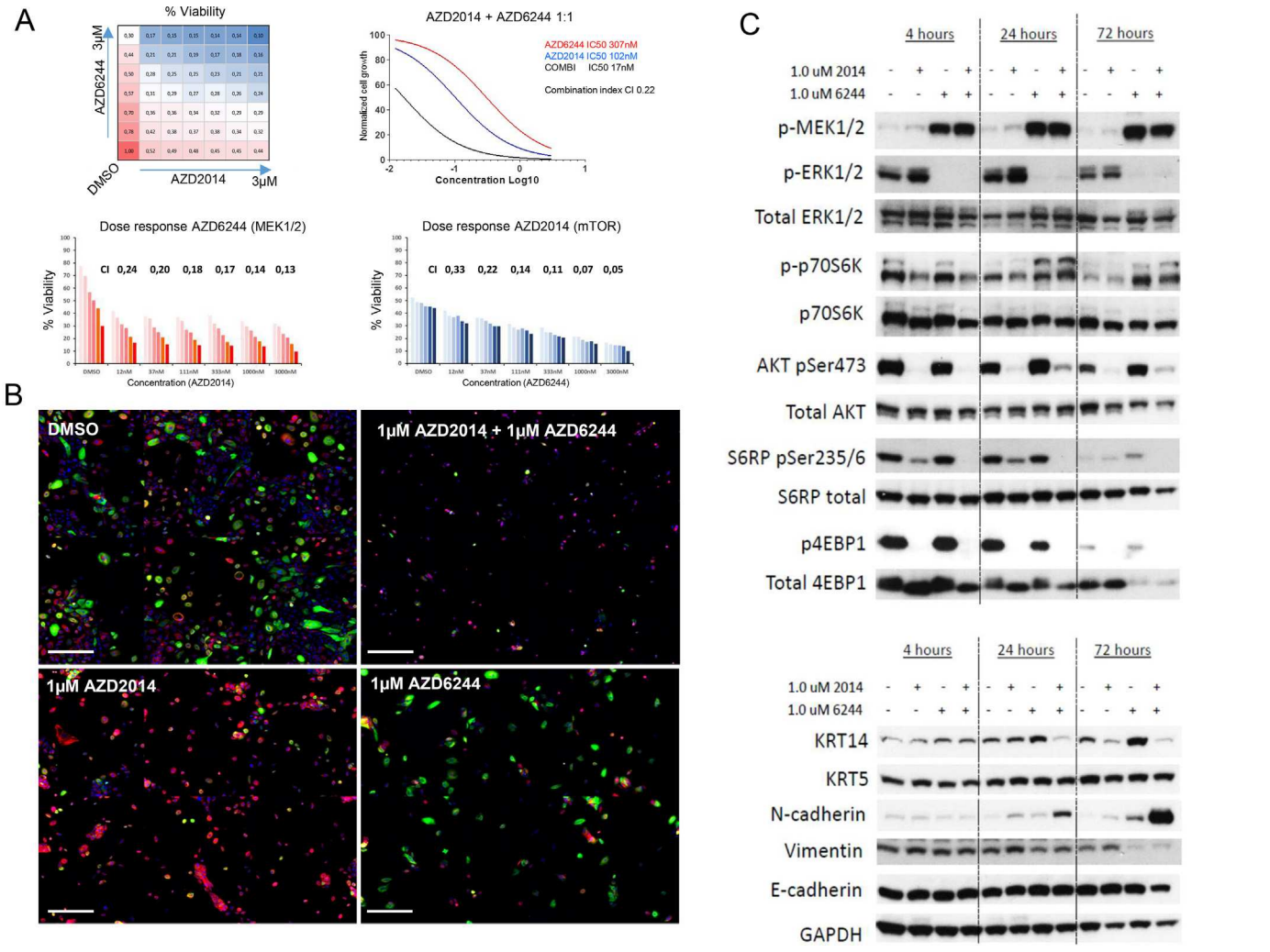

Fig. 4. Drug combinations in EMC. (A) Dose–response matrix of percent of viability at increasing doses of AZD2014 (mTOR inhibitor) and AZD6244 (MEK inhibitor). The measured CI50 combination index of AZD2014 and AZD6244 was 0.22. Lower panel, comparison of growth inhibition dose responses of AZD2014 and AZD6244 with fixed concentration of the other drug. (B) Immunofluorescent staining of EMC cells with KRT19 (red) and KRT14 (green) following 96-h treatment with single agent AZD2014, AZD6244, combination of the two and control DMSO treated cells. Bar 50 µm. C, EMC cells were treated with DMSO (−), 1000 nmol/L AZD2015, 1000 nmol/L AZD6244, or the combination for 4, 24 and 72 h, and phosphorylation (p) and total protein levels of indicated markers was assessed. GAPDH was assessed as a loading control.

Table 1. Key oncogenic aberrations discovered in the patient tumor cells.

Gene	Effect	Impact	Codon_Change	Exon	AA_Change
ARID1B	CODON_DELETION	MODERATE	caggcg/cag	1	QA456Q
ATR	FRAME_SHIFT	HIGH	ata/aAta	10	I774N
CDK12	FRAME_SHIFT	HIGH	–/–	14	−1443
ERBB4	NON_SYNONYMOUS_CODING	MODERATE	gTg/gGg	8	V298G
HRAS	NON_SYNONYMOUS_CODING	MODERATE	Ggt/Cgt	2	G13R
MAPK1	CODON_CHANGE_PLUS_CODON_DELETION	MODERATE	gcgggc/ggc	1	AG7G
NANOG	NON_SYNONYMOUS_CODING	MODERATE	Act/Cct	4	T281P
NANOG	STOP_GAINED	HIGH	Caa/Taa	4	Q301*
NOTCH2	FRAME_SHIFT	HIGH	–/–	1	−6
PIK3R1	CODON_CHANGE_PLUS_CODON_DELETION	MODERATE	cgagaa/caa	10	RE461Q
PIK3R1	STOP_GAINED	HIGH	tTa/tAa	5	L244*
RPTOR	NON_SYNONYMOUS_CODING	MODERATE	Tgg/Ggg	33	W1313G

new biopsy sample was retrieved from this lesion. Tumor cells from the new lesion stained positive for HER2 without detection of amplification of the HER2/ERBB2 gene with CISH. Based on results from the initial *ex vivo* screen showing moderate response of the patient's tumor cells to inhibition of EGFR/HER2 axis and high protein level HER2 staining, a new treatment attempt was made using combination of trastuzumab–em-

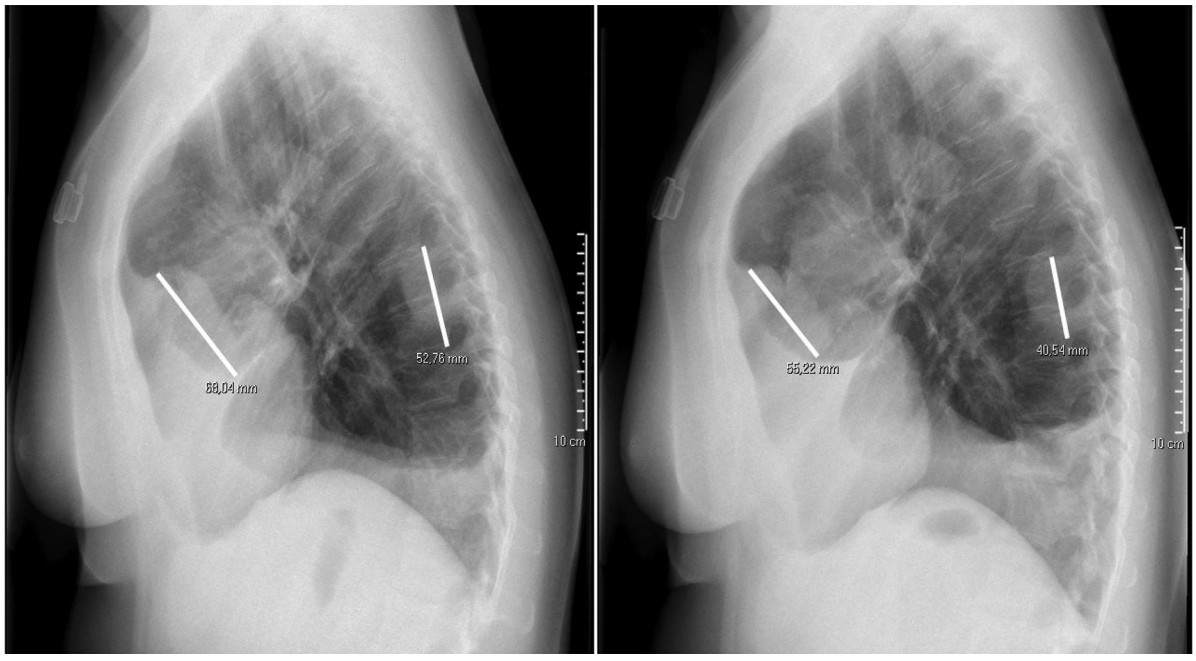

Fig. 5. Clinical response to Everolimus (mTOR inhibitor) therapy. Following four weeks of treatment with 10 mg/day Everolimus the intrapulmonary metastasis lesions showed ∼25% reduction in diameter.

tansine (Kadcyla) and Lapatinib. Patient reported that disease lesions were less painful during the therapy; however, whole-body CT scans showed unequivocal progression of the disease at multiple disease locations. At that point, patient was switched to best palliative care and received radiation therapy to painful disease lesions. She succumbed to disease shortly after stopping of active treatment.

Conclusions

We report here the first described *ex vivo* study and clinical use of drug efficacy testing in epithelial myoepithelial carcinoma. In an effort to model therapeutic options for a patient with an aggressive metastatic EMC, we performed a high content image-based *ex vivo* drug screening using tumor cells freshly isolated from a lung metastasis coarse needle biopsy. The analysis yielded dose and target dependent cytotoxic profiles for tens of drugs which could be linked to genetic features of the patient's cancer cells. Moreover, the analysis identified significant differential drug sensitivity between the sub-cell lineages composing the tumor tissue highlighting the importance of lineage heterogeneity of tumors contributing to therapy sensitivity. Especially targeted therapeutics could be linked with differential pathway dependency in the epithelial and myoepithelial tumor cells. These included a mTOR inhibitors, MEK inhibitors, HDAC inhibitors and topoisomerase inhibitors. The lineage specific interrogation of drug induced growth inhibition also highlighted the importance of implementing growth rate corrected dose response measurements, a feature largely neglected in the drug screening approaches published to date.

In summary, by interrogating patient-derived cells in this *ex vivo* study we identify mTOR and MEK inhibitors as potential therapeutic options that could be considered as alternative treatment regimens for patients with a metastatic epithelial myoepithelial carcinoma. These results also suggest that the lineage heterogeneity in epithelial myoepithelial salivary gland cancer can present a partial outlet to targeted therapy and that lineage heterogeneity could be considered as a predictive biomarker when selecting among pathway targeted treatment options that are known to display lineage selectivity also in other cancers [29].

Declarations of interest

Dr Juha K. Rantala is the founder and CEO of Misvik Biology Ltd. The authors declare no potential conflicts of interest.

Acknowledgements

We would like to thank the patient and the family with whom this study is connected and the personnel of the Central Finland Health Care District, JyvÌskylÌ Medical Centre Oncology Department. The ODM-207 bromodomain inhibitor was provided to the study kindly by Dr. Anu Moilanen (Orion, Turku, Finland).

Funding

This work has been supported in part by AZ-SLL-KI open innovation grant #18122013. The funding body had no input in the design of the study, collection, analysis or interpretation of the data.

Appendix A. Supplementary data

Supplementary data to this article can be found online at https://doi.org/10.1016/j.neo.2020.06.007.

References

1. Donath K, Seifert G, Schmitz R. Diagnosis and ultrastructure of the tubular carcinoma of salivary gland ducts: epithelial-myoepithelial carcinoma of the intercalated ducts [in German]. *Virchows Arch A Pathol Pathol Anat* 1972;**356**:16–31.
2. VÄzquez A, Patel TD, D'Aguillo CM, Abdou RY, Farver W, Baredes S, et al. Epithelial-myoepithelial carcinoma of the salivary glands: an analysis of 246 cases. *Otolaryngol Head Neck Surg* 2015;**153**(4):569–74.
3. Senis-Segarra L, Sahuquillo-Arce E, Davo R, Hamad-Arcis P, Floria-Garcia MC, Baquero MC. Salivary gland epithelial-myoepithelial carcinoma: behaviour, diagnosis and treatment. *Med Oral* 2002;**7**:391–5.

4. Seethala RR, Barnes EL, Hunt JL. Epithelial-myoepithelial carcinoma: a review of the clinicopathologic spectrum and immunophenotypic characteristics in 61 tumors of the salivary glands and upper aerodigestive tract. *Am J Surg Pathol* 2007;**31**:44–57.
5. Shinozaki A, Nagao T, Endo H, Kato N, Hirokawa M, Mizobuchi K, et al. Sebaceous epithelial-myoepithelial carcinoma of the salivary gland: clinicopathologic and immunohistochemical analysis of 6 cases of a new histologic variant. *Am J Surg Pathol* 2008;**32**(6):913–23.
6. Venook AP, Tseng A, Meyers FJ, Silverberg I, Boles R, Fu KK, Jacobs CD. Cisplatin, doxorubicin, and 5-fluorouracil chemotherapy for salivary gland malignancies: a pilot study of the Northern California Oncology Group. *J Clin Oncol* 1987;**5**:951–5.
7. Airoldi M, Pedani F, Succo G, Gabriele AM, Ragona R, Marchionatti S, Bumma C. Phase II randomized trial comparing vinorelbine versus vinorelbine plus cisplatin in patients with recurrent salivary gland malignancies. *Cancer (Phila.)* 2001;**91**:541–7.
8. Jennings T, Li Y, Pinto H, Kies M, Mansour E, Foratsiere A. Phase II trial of paclitaxel in advanced or metastatic salivary gland malignancies: an Eastern Cooperative Oncology Group Study. *Proc Am Soc Clin Oncol* 2001;**20**:236a.
9. Prior IA, Lewis PD, Mattos C. A comprehensive survey of Ras mutations in cancer. *Cancer Res* 2012;**72**(10):2457–67.
10. Cros JF, Blons H, Sbidian E, Tartour E, Hans S, Brasnu D, et al. Expression and prognostic significance of directed therapy targets and mutational analysis of the EGFR pathway in malignant salivary gland tumors. *J Clin Oncol* 2012;**30**:5554.
11. Chiosea SI, Miller M, Seethala RR. HRAS mutations in epithelial-myoepithelial carcinoma. *Head and Neck Pathol* 2014;**8**:146–50.
12. Kettunen K, BostrÎm PJ, Lamminen T, et al. Personalized drug sensitivity screening for bladder cancer using conditionally reprogrammed patient-derived cells. *Eur Urol* 2019;**76**(4):430–4.
13. Lehtomaki KI, Lahtinen LI, Rintanen N, et al. Clonal evolution of MEK/MAPK pathway activating mutations in a metastatic colorectal cancer case. *Anticancer Res* 2019;**39**(11):5867–77.
14. Arjonen A, MÌkelÌ R, HÌrmÌ V, et al. Image-based ex vivo drug screen to assess targeted therapies in recurrent thymoma. *Lung Cancer* 2020;**145**:27–32.
15. Billingham L, Malottki K, Steven N. Research methods to change clinical practice for patients with rare cancers. *Lancet Oncol* 2016;**17**:e70–80.
16. Shannon CE, Weaver W. *The Mathematical Theory of Communication*. University of Illinois Press; 1963.
17. Chou TC. Drug combination studies and their synergy quantification using the Chou-Talalay method. *Cancer Res* 2010;**70**:440–6.
18. Labarge MA, Garbe JC. Stampfer MR. Processing of human reduction mammoplasty and mastectomy tissues for cell culture. *J Vis Exp* 2013(71).
19. Hafner M, Heiser LM, Williams EH, Niepel M, Wang NJ, Korkola JE, et al. Quantification of sensitivity and resistance of breast cancer cell lines to anti-cancer drugs using GR metrics. *Sci Data* 2017;**4** 170166.
20. Neumann B, Walter T, HÅrichÅ JK, Bulkescher J, Erfle H, Conrad C, et al. Phenotypic profiling of the human genome by time-lapse microscopy reveals cell division genes. *Nature* 2010;**464**(7289):721–7.
21. Gujral TS, Karp RL, Finski A, Chan M, Schwartz PE, MacBeath G, Sorger P. Profiling phospho-signaling networks in breast cancer using reverse-phase protein arrays. *Oncogene* 2013;**32**:3470–6.
22. Serra V, Markman B, Scaltriti M, Eichhorn PJ, Valero V, et al. NVPBEZ235, a dual PI3K/mTOR inhibitor, prevents PI3K signaling and inhibits the growth of cancer cells with activating PI3K mutations. *Cancer Res* 2008;**68**:8022–30.
23. Chapuis N, Tamburini J, Green AS, Vignon C, Bardet V, et al. Dual inhibition of PI3K and mTORC1/2 signaling by NVP-BEZ235 as a new therapeutic strategy for acute myeloid leukemia. *Clin Cancer Res* 2010;**16**:5424–35.
24. Duncan JS, Whittle MC, Nakamura K, Abell AN, Midland AA, Zawistowski JS, et al. Dynamic reprogramming of the kinome in response to targeted MEK inhibition in triple-negative breast. *Cancer Cell* 2012;**149**:307–21.
25. Cheung LW, Yu S, Zhang D, Li J, Ng PK, Panupinthu N, et al. Naturally occurring neomorphic PIK3R1 mutations activate the MAPK pathway, dictating therapeutic response to MAPK pathway inhibitors. *Cancer Cell* 2014;**26**(4):479–94.
26. Kiessling MK, Curioni-Fontecedro A, Samaras P, Atrott K, Cosin-Roger J, Lang S, et al. Mutant HRAS as novel target for MEK and mTOR inhibitors. *Oncotarget* 2015;**6**(39):42183–96.
27. Cheung LW, Mills GB. Targeting therapeutic liabilities engendered by PIK3R1 mutations for cancer treatment. *Pharmacogenomics* 2016;**3**:297–307.
28. Dela Cruz FS, Diolaiti D, Turk AT, Rainey AR, Ambesi-Impiombato A, Andrews SJ, et al. A case study of an integrative genomic and experimental therapeutic approach for rare tumors: identification of vulnerabilities in a pediatric poorly differentiated carcinoma. *Genome Med* 2016;**8**(1):116.
29. Risom T, Langer EM, Chapman MP, Rantala J, Fields AJ, Boniface C, et al. Differentiation-state plasticity is a targetable resistance mechanism in basal-like breast cancer. *Nat Commun* 2018;**9**(1):3815.